

Article

# Heterogenous Preparations of Solution-Processable Cobalt Phthalocyanines for Carbon Dioxide Reduction Electrocatalysis

Elahe Tajbakhsh <sup>1</sup>, Declan McKearney <sup>1</sup>, Daniel B. Leznoff <sup>1,\*</sup> and Jeffrey J. Warren <sup>1,\*</sup> 

Department of Chemistry, Simon Fraser University, 8888 University Drive, Burnaby, BC V5A 1S6, Canada

\* Correspondence: dleznoff@sfu.ca (D.B.L.); jjwarren@sfu.ca (J.J.W.)

**Abstract:** The development and implementation of technology that can capture and transform carbon dioxide (CO<sub>2</sub>) is of ongoing interest. To that end, the integration of molecular electrocatalysts into devices is appealing because of the desirable features of molecules, such as the ability to modify active sites. Here, we explore how the identity of the aliphatic group in 1,4,8,11,15,18,22,25-octaalkoxyphthalocyanine cobalt(II) affects the catalytic behavior for heterogeneous CO<sub>2</sub> reduction electrocatalysis. The alkyl R-groups correspond to *n*-butoxy, *sec*-butoxy, and 2-ethylhexoxy. All of the catalysts are soluble in organic solvents and are readily solution-processed. However, the larger 2-ethylhexoxy group showed solution aggregation behavior at concentrations  $\geq 1$  mM, and it was, in general, an inferior catalyst. The other two catalysts show comparable maximum currents, but the octa *sec*-butoxy-bearing catalyst showed larger CO<sub>2</sub> reduction rate constants based on foot-of-the-wave analyses. This behavior is hypothesized to be due to the ability of the *sec*-butoxy groups to eliminate the ability of the alkoxy oxygen to block Co Sites via ligation. CO<sub>2</sub> reduction activity is rationalized based on solid-state structures. Cobalt(II) phthalocyanine and its derivatives are known to be good CO<sub>2</sub> reduction catalysts, but the results from this work suggest that straightforward incorporation of bulky groups can improve the processability and per site activity by discouraging aggregation.

**Keywords:** carbon dioxide reduction; cobalt; phthalocyanines; heterogeneous electrocatalysis; catalyst design



check for updates

**Citation:** Tajbakhsh, E.; McKearney, D.; Leznoff, D.B.; Warren, J.J. Heterogenous Preparations of Solution-Processable Cobalt Phthalocyanines for Carbon Dioxide Reduction Electrocatalysis. *Inorganics* **2023**, *11*, 43. <https://doi.org/10.3390/inorganics11010043>

Academic Editor: Torben R. Jensen

Received: 16 December 2022

Revised: 7 January 2023

Accepted: 11 January 2023

Published: 15 January 2023



**Copyright:** © 2023 by the authors. Licensee MDPI, Basel, Switzerland. This article is an open access article distributed under the terms and conditions of the Creative Commons Attribution (CC BY) license (<https://creativecommons.org/licenses/by/4.0/>).

## 1. Introduction

The development of catalyst technology that can convert carbon dioxide (CO<sub>2</sub>) to useful reduced products is of great interest in the ongoing fight against climate change [1–4]. Promising capture platforms have emerged [5,6], but finding catalysts that can convert the captured CO<sub>2</sub> to desirable products remains a challenge. One approach that has received a great deal of attention is using electrochemical reduction to convert CO<sub>2</sub> to fuels, value-added chemicals, and/or fuel precursors (e.g., carbon monoxide, CO; methanol, CH<sub>3</sub>OH; ethylene, C<sub>2</sub>H<sub>4</sub>; etc.) [2–4]. In particular, the utilization of renewable electricity to drive reactions is desirable. Many CO<sub>2</sub> reduction products are possible, including CO, CH<sub>3</sub>OH, formic acid (HCOOH), formaldehyde (H<sub>2</sub>CO), methane (CH<sub>4</sub>), and higher order C-C-coupled products (ethane, ethylene, etc.) [7]. For example, CO-producing CO<sub>2</sub> electrolyzers can use metallic catalysts, such as copper and gold [7–9], which also give rise to attractive products (e.g., C-C-coupled). A drawback of metal electrodes is that they are less tunable/modifiable in the same ways as molecular electrocatalysts. Thus, strategies are needed that connect the desirable features of molecular and materials electrocatalysts for CO<sub>2</sub> reduction.

Large heterogeneous catalyst assemblies with good current densities are needed for practical applications [4–6]. One recent analysis highlights the importance of scale in the CO<sub>2</sub> conversion problem [5]. An air-to-barrel methanol plant that produces 10,000 tons of methanol per day (a benchmark for large-scale application) is required to have a catalyst

area of 175,000 m<sup>2</sup> (0.175 km<sup>2</sup>) based on current technology. This requirement has led to many strategies to produce catalyst assemblies with large surface areas, as outlined below. In particular, research on catalysts derived from molecular cobalt complexes, which have long been known to electrocatalytically reduce CO<sub>2</sub>, are of continuing interest [10–15].

One approach to address the need for large catalyst areas is to focus on improving current density of catalysts by increasing the density of active sites. This can be achieved, for instance, by making extended structured materials, such as covalent organic frameworks [16,17]. Improvements to mass transport and electron mobility are ongoing, as highlighted in a recent review [18]. Another strategy is to disperse catalysts directly on conductive supports, such as carbon. This strategy also can increase the intrinsic per site by considering dispersion. To that end, a recent investigation of the known [10,19–21] CO<sub>2</sub> reduction catalyst cobalt(II) phthalocyanine (PcCo) showed how dispersion of the catalyst on oxygen-functionalized carbon affects operating currents and selectivity [22]. Using Nafion-suspended inks on carbon, the highest turnover frequencies (ca. 10<sup>2</sup> s<sup>-1</sup>) were observed for the lowest catalyst concentrations (10<sup>-11</sup> mol cm<sup>2</sup>), though the more highly dispersed preparations also showed a greater degree of proton reduction. A related strategy is the immobilization of PcCo on multi-walled carbon nanotubes, which shows good selectivity for production of CO or CH<sub>3</sub>OH, depending on the preparation and operational conditions [15,23–25]. Importantly, the above preparations commonly involve dispersion of PcCo in mixtures of organic solvent, Nafion, and the carbon substrate. In these systems, the absolute Co loading can be determined using different materials' characterization techniques, but the specific interactions between molecules in any aggregates is more difficult to assess. Preparations of carbon materials using soluble cobalt catalysts can yield materials with good CO<sub>2</sub> reduction activity [26], and this has been assessed in lab-scale devices for solubilized PcCo and some solution processable derivatives [27,28].

An important challenge associated with using unfunctionalized Pc-metal catalysts is that they are sparingly soluble. For example, the maximum solubility of the unsubstituted PcCo is under 1 nM in most solvents [29]. In most cases, unsubstituted MPcs can form H (face-to-face) or J (edge-to-edge) aggregates, further limiting solubility and often blocking active sites [30]. There are examples of successful solubilization and dispersion of PcCo from *N,N*-dimethylformamide solutions onto carbon nanotubes [15,25,31]. An approach that offers other avenues to suppress aggregation and tune catalytic properties is to change the chemical structure of the compounds. Functionalizing metallophthalocyanines with different ring-substituents [32,33] and/or axial groups [34] coordinated by the metal center can protect the  $\pi$ -conjugated chromophores from unwanted intermolecular interactions. The increase in solubility also results in molecules that can be solution-processed, facilitating their incorporation into materials.

Herein, we explore the CO<sub>2</sub> reduction properties of heterogeneous preparations of a closely related series of organic-solvent soluble cobalt phthalocyanines (Figure 1) that include bulky aliphatic groups to facilitate solution processing and discourage aggregation that can block, or otherwise inactivate, the active sites. This work is related to the recent investigation of CO<sub>2</sub> reduction using 1,4,8,11,15,18,22,25-octaalkoxyphthalocyanine cobalt(II) dispersed on graphene [35]. In that work, dispersion was shown to increase the per site CO<sub>2</sub> reduction activity of cobalt. In the present work, we probe how the addition of different bulky aliphatic groups to PcCo affects the solution processing, aggregation, and observed CO<sub>2</sub> reduction electrocatalytic properties.

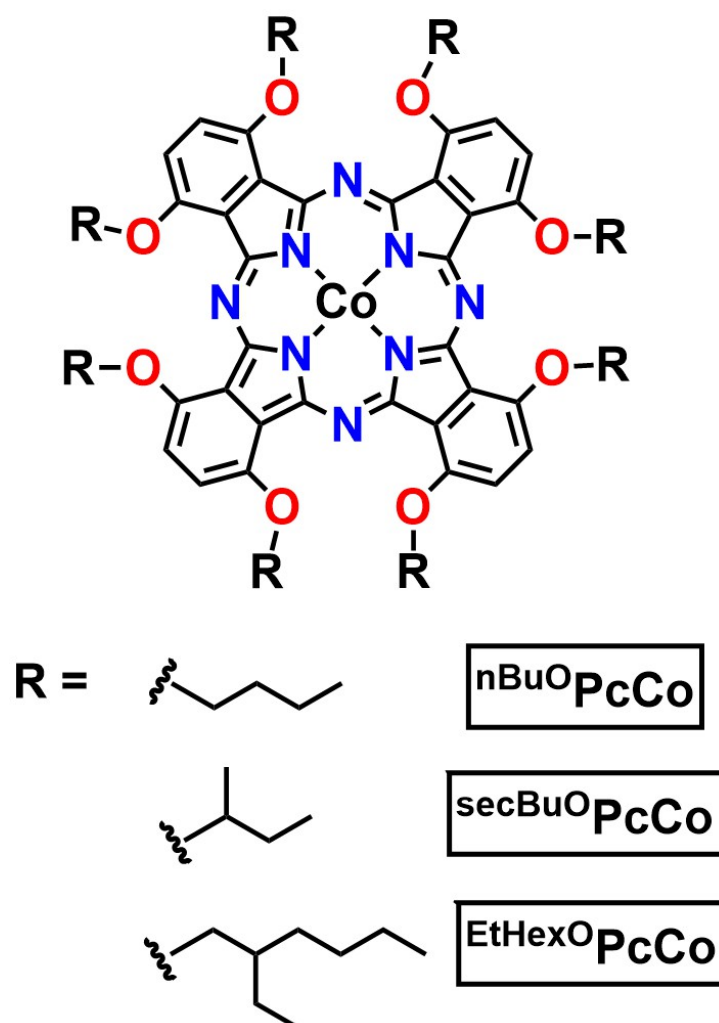


**Figure 1.** Structures of 1,4,8,11,15,18,22,25-octaalkoxyphthalocyanine cobalt(II) ( $^{\text{R}}\text{O}\text{PcCo}$ ) electrocatalysts (R = n-butyl, sec-butyl, and 2-ethylhexyl).

## 2. Results

### 2.1. Design and Synthesis of $^{\text{R}}\text{O}\text{PcCo}$

The three 1,4,8,11,15,18,22,25-octaalkoxyphthalocyanine cobalt(II) complexes ( $^{\text{R}}\text{O}\text{PcCo}$ ) investigated here (Figure 1) were prepared by alkylation of 2,3-dicyanohydroquinone, followed by lithium-templated cyclization in ROH solvent (R = n-butyl, sec-butyl and 2-ethylhexyl) and addition of acetic acid to form the free ligand [36]. Note that, in the cyclization step, it is necessary to use the same alcohol as the R-group being installed in order to prevent substituent exchange that leads to asymmetric compounds [37]. Metalation was carried out using  $\text{Co}(\text{CH}_3\text{COO})_2$  at 80 °C in DMF. The known octa-n-butoxy-substituted PcCo (denoted  $^{\text{nBuO}}\text{PcCo}$ ) is a previously reported heterogeneous  $\text{CO}_2\text{RR}$  catalyst [19]. Related alkoxy-substituted metallophthalocyanines are soluble in a range of solvents [36, 38,39]. The structurally related octa-sec-butoxy- and octa-2-ethylhexylbutoxy-substituted phthalocyanines ( $^{\text{secBuO}}\text{PcCo}$  and  $^{\text{EtHexO}}\text{PcCo}$ , respectively), also are soluble in common organic solvents, such as toluene, dichloromethane, and tetrahydrofuran. In both cases, the bulky alkyl groups are designed to prevent  $\pi$ -stacking, where the bulkier  $^{\text{EtHexO}}\text{PcCo}$  is designed to discourage any interaction between Co centers or the  $\pi$ -systems of the Pc ligands via the steric bulk of the alkoxy groups.

## 2.2. Solution Aggregation of $^{\text{RO}}\text{PcCo}$ Compounds

The solution properties of the  $^{\text{RO}}\text{PcCo}$  compounds were investigated in toluene. While the parent PcCo can be solubilized to some extent in *N,N*-dimethylformamide [23,25], solubility in more volatile solvents would aid solution processing of materials. UV-visible spectra were obtained using  $^{\text{RO}}\text{PcCo}$  concentrations of 1 mM, 0.18 mM, 32  $\mu\text{M}$ , and 5  $\mu\text{M}$ . The UV-vis spectra were analyzed using the Beer–Lambert law and deviations from the predicted linear concentration–absorbance relationship were taken as an indication of solution aggregation [40–42]. Based on this, for each compound, the intercept, slope and correlation coefficient ( $R^2$ ) were analyzed in all the wavelengths with absorbance values < 2. Note that the optical spectra shown in the Supporting Information (Figure S2) include all absorbance values, not just those below 2. These values were not used in our analysis and are simply shown for completeness. Based on the results,  $^{\text{nBuO}}\text{PcCo}$  does not aggregate at the concentrations tested. For  $^{\text{secBuO}}\text{PcCo}$ , there are small changes to the Soret bands (ca. 400 nm), which could suggest a small degree of aggregation. In contrast,  $^{\text{EtHexO}}\text{PcCo}$  showed distinctly irregular absorbance peak shapes as the concentration was increased to 1 mM. Such behavior suggests a greater degree of aggregation for this complex at concentrations > 0.18 mM.

## 2.3. Solution Electrochemistry

The solution electrochemistry of each catalyst was first explored in benzonitrile solvent (with 0.1 M  $^{\text{nBu}}_4\text{NPF}_6$  electrolyte) at 0.2 mM concentration under an Ar atmosphere. Two closely spaced, reversible waves are observed near  $-0.1$  V versus  $\text{Cp}_2\text{Fe}^{+/0}$  (Table 1). Voltammograms are set out in the Supporting Information, including wide (Figure S3) and narrow (Figures S4 and S5) scan ranges. Related voltammograms, in MeCN solvent, of  $^{\text{nBuO}}\text{PcCo}$  also show some unassigned features [43]. The origin of the additional waves is not known, but differently solvent-ligated forms of the catalysts could be present [38]. Likewise, based on the above results, some degree of aggregation may occur in solution or at the electrode surface, resulting in the minor waves [31]. The largest observed waves occur at potentials consistent with the Co(III/II) couple [43]. A second reversible wave is observed between  $-0.9$  and  $-1$  V. The observed potentials are similar to those reported for  $^{\text{nBuO}}\text{PcCo}$  in  $\text{CH}_2\text{Cl}_2$  solvent [43].

**Table 1.** Homogeneous  $^{\text{RO}}\text{PcCo}$  reduction potentials in benzonitrile.

Compound	$E_{1/2}[^{\text{RO}}\text{PcCo}^{+/0}]^a$	$E_{1/2}[^{\text{RO}}\text{PcCo}^{0/-}]^a$
$^{\text{nBuO}}\text{PcCo}$	$-0.08$	$-0.97$
$^{\text{secBuO}}\text{PcCo}$	$-0.14$	$-0.94$
$^{\text{EtHexO}}\text{PcCo}$	$-0.14$	$-0.94$

<sup>a</sup> Potentials in V versus  $\text{Cp}_2\text{Fe}^{+/0}$ .

## 2.4. Heterogeneous Electrochemistry under Argon

Solutions of  $^{\text{RO}}\text{PcCo}$  with concentrations of 1 mM, 0.18 mM, 32  $\mu\text{M}$ , 5  $\mu\text{M}$ , 1.0  $\mu\text{M}$ , and 0.18  $\mu\text{M}$  in toluene were deposited on basal plane graphite (BPG) electrodes and analyzed using cyclic voltammetry (CV). In each case, 5  $\mu\text{L}$  of each solution was deposited, which corresponds to loadings ranging from  $5.6 \times 10^{-8}$  mol  $\text{cm}^{-2}$  (using a 1 mM solution) to  $1.0 \times 10^{-11}$  mol  $\text{cm}^{-2}$  (using a 0.18  $\mu\text{M}$  solution). CVs were collected in 0.1 M KCl electrolyte (pH 4.5) that was sparged with argon or  $\text{CO}_2$  (see below). A wide range of electrolytes has been investigated for PcCo-catalyzed  $\text{CO}_2$  reduction [44]. KCl was chosen here to allow for the clearest comparison between inert and  $\text{CO}_2$  atmospheres. The pH was adjusted to 4.5 because that is the pH we measure for an aqueous solution under 1 atm  $\text{CO}_2$ .

The CVs of  $^{\text{nBuO}}\text{PcCo}$  showed a feature at  $-0.26$  V versus NHE, consistent with a reported value for this compound under similar conditions [45]. Weak waves at similar potentials also are observed in graphene +  $^{\text{RO}}\text{PcCo}$  conjugates [35]. The wave at  $-0.26$  V was assigned to the Co(III/II) redox couple. In contrast to  $^{\text{nBuO}}\text{PcCo}$ , CVs of  $^{\text{secBuO}}\text{PcCo}$

and  $\text{EtHexOPcCo}$  only showed discernable waves under Ar at the highest loading (from 1 mM solution). The Co(III/II) wave appeared at  $-0.17$  V for  $\text{secBuOPcCo}$  and at  $-0.20$  V for  $\text{EtHexOPcCo}$ . Representative voltammograms at selected concentrations are set out in Figure 2 and a full series of CVs is available in the Supporting Information (Figures S6–S31). The corresponding data for scans under  $\text{CO}_2$  (Figure 2 and Figure S32–S42) are discussed below. In all cases, the peak currents for scans under Ar are linear with respect to the scan rate (Figures S43–S61 and S63), suggesting that each  $\text{ROpCo}$  is adsorbed.

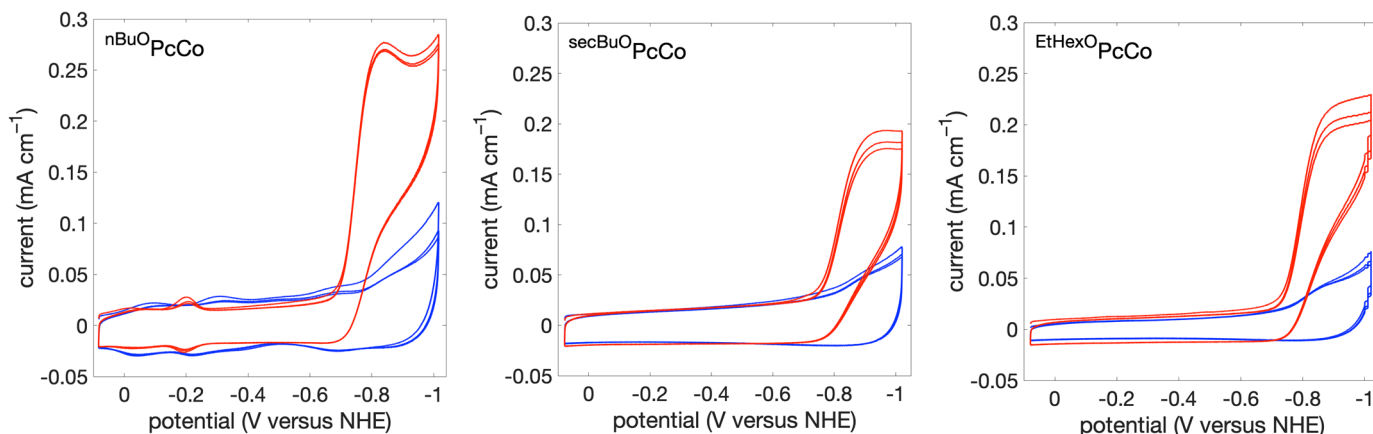


**Figure 2.** Representative cyclic voltammograms of drop cast  $\text{ROpCo}$  under 1 atm argon (blue) and under 1 atm  $\text{CO}_2$  (red). Traces were recorded at  $100 \text{ mV s}^{-1}$ . The deposited concentrations were 1 mM ( $\text{nBuOPcCo}$ ), 0.18 mM ( $\text{secBuOPcCo}$ ), and 0.18 mM ( $\text{EtHexOPcCo}$ ).

The electroactive Co concentration was assessed at each loading using CV or differential pulse voltammetry (DPV) experiments. These values are tabulated in Table 2 and Table S1. In some cases, in particular at the lowest  $\text{ROpCo}$  loadings, there was no detectable electrochemical response at the Co(III/II) potential, even when using the sensitive DPV technique (Figure S61). In general, only a fraction of the deposited complexes are electroactive. This is a common observation for graphite-adsorbed porphyrins [46,47], and it is possible that such behavior indicates that the deposited complexes behave like metallic electrodes [48]. For the substituted  $\text{ROpCo}$  studied here, there is a correlation between the bulk of the alkoxy group and the magnitude of the observed current at the first reduction, where the larger  $\text{secBuOPcCo}$  and  $\text{EtHexOPcCo}$  have weaker currents.

### 2.5. Heterogeneous Electrochemistry under Carbon Dioxide

Drop cast  $\text{ROpCo}$  on BPG electrodes were again prepared using solutions of  $\text{ROpCo}$  at 1 mM, 0.18 mM, 32  $\mu\text{M}$ , 5  $\mu\text{M}$ , 1.0  $\mu\text{M}$ , and 0.18  $\mu\text{M}$  concentrations. CVs were then collected in  $\text{CO}_2$ -saturated aqueous 0.1 M KCl, pH 4.5. The deposition concentrations were chosen to give final loadings that align with a range of concentrations tested in a related study [22] and those net cobalt concentrations used in preparations with carbon nanotubes (ca.  $10^{-8} \text{ mol cm}^{-1}$ ) [23,24] or polyvinylpyridine (ca.  $10^{-9} \text{ mol cm}^{-1}$ ) [49]. In all cases, catalytic waves for our electrode preparations were observed, with onset potentials near  $-0.7$  V versus NHE (Figure 2 and Figure S6–S41). These onset potentials (overpotentials) are slightly more negative (ca. 50 to 100 mV) than for heterogeneous preparations of unfunctionalized  $\text{PcCo}$  [22,23,49], which can be attributed to the electron-donating alkoxy groups in  $\text{ROpCo}$ . The relative increase in current was between 5- and 20-fold, depending on the complex and the loading. These comparisons are set out in Figure 3. Data for other scans at each deposition concentration (in triplicate) are set out in the Supporting Information (Figures S6–S41).

The stability of the drop-cast catalysts was probed with repeated CV scans and controlled potential electrolysis (CPE) experiments (Figures S66 and S67). The traces of repeated CV scans are nearly superimposable and CPE traces of replicate experiments showed mod-

est decreases in current density over a 2 h CPE experiment. Taken together, these results suggest that drop-cast preparations of the  $^{\text{RO}}\text{PcCo}$  complexes can be stable under catalytic conditions. Long-term, *in operando* testing and more advanced materials' characterization are still necessary to fully understand the stability of the catalyst preparations.

**Table 2.** Summary of electrochemical data for  $^{\text{RO}}\text{CoPc}$  complexes.

nBuOPcCo				
Deposition Solution Concentration	Loading ( $\text{mol cm}^{-2}$ )	Average $\Gamma_{\text{cat}}$ ( $\text{mol cm}^{-2} \times 10^{-13}$ )	$k_{\text{FOW}}$ ( $\text{s}^{-1}$ )	Average CPE Current Density ( $\mu\text{A cm}^{-2}$ )
1000 $\mu\text{M}$	$5.5 \times 10^{-8}$	$3.2 \pm 0.6$	$59 \pm 20$	76.7
180 $\mu\text{M}$	$9.9 \times 10^{-9}$	$4.3 \pm 2.1$	$410 \pm 290$	83.0
32 $\mu\text{M}$	$1.8 \times 10^{-9}$	$4.3 \pm 1.7$	$420 \pm 70$	153
5 $\mu\text{M}$	$2.8 \times 10^{-10}$	$7.1 \pm 2.9$	$190 \pm 60$	73.6
1 $\mu\text{M}$	$5.6 \times 10^{-11}$	$3.8 \pm 0.3$	$220 \pm 90$	90.3
0.18 $\mu\text{M}$	$1 \times 10^{-11}$	$0.23 \pm 0.04$	$930 \pm 150$	8.7
secBuOPcCo				
1000 $\mu\text{M}$	$5.5 \times 10^{-8}$	$2.3 \pm 0.6$	$4100 \pm 1000$	26.5
180 $\mu\text{M}$	$9.9 \times 10^{-9}$	$5.5 \pm 0.1$	$810 \pm 60$	25.4
32 $\mu\text{M}$	$1.8 \times 10^{-9}$	$3.7 \pm 0.7$	$550 \pm 130$	51.5
5 $\mu\text{M}$	$2.8 \times 10^{-10}$	$1.4 \pm 0.2$	$2300 \pm 1200$	58.4
1 $\mu\text{M}$	$5.6 \times 10^{-11}$	– <sup>a</sup>	– <sup>a</sup>	66.8
0.18 $\mu\text{M}$	$1 \times 10^{-11}$	– <sup>a</sup>	– <sup>a</sup>	56.7
EtHexOPcCo				
1000 $\mu\text{M}$	$5.5 \times 10^{-8}$	$0.60 \pm 0.12$	$2000 \pm 570$	135
180 $\mu\text{M}$	$9.9 \times 10^{-9}$	$3.6 \pm 1.5$	$1800 \pm 540$	26.5
32 $\mu\text{M}$	$1.8 \times 10^{-9}$	$3.1 \pm 0.5$	$730 \pm 120$	76.3
5 $\mu\text{M}$	$2.8 \times 10^{-10}$	$1.6 \pm 0.3$	$1300 \pm 160$	66.2
1 $\mu\text{M}$	$5.6 \times 10^{-11}$	– <sup>a</sup>	– <sup>a</sup>	48.6
0.18 $\mu\text{M}$	$1 \times 10^{-11}$	– <sup>a</sup>	– <sup>a</sup>	57.9

<sup>a</sup> Electroactive concentrations were not calculated due to very weak observed currents; this also precludes calculation of  $k_{\text{FOW}}$ .

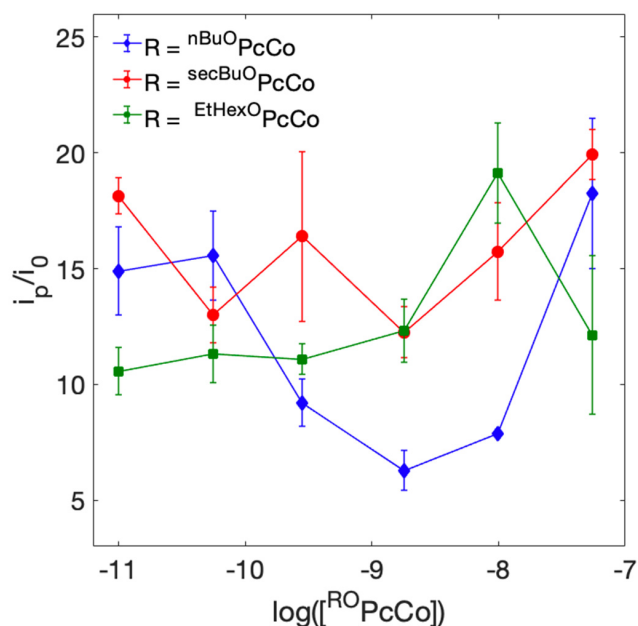


**Figure 3.** Ratio of current in the absence of  $\text{CO}_2$  ( $i_0$ ) to catalytic peak currents under 1 atm  $\text{CO}_2$  ( $i_p$ ) at each catalyst loading. The x-axis is the logarithm of the deposition concentration in  $\text{mol cm}^{-2}$ . Blue diamonds =  $^{\text{nBuO}}\text{PcCo}$ , red circles =  $^{\text{secBuO}}\text{PcCo}$ , and green squares =  $^{\text{EtHexO}}\text{PcCo}$ .

Finally, the headspace of CPE experiments was analyzed using gas chromatography. CO was the only detected product. However, due to our limits of detection, we cannot discount some reduction of protons to H<sub>2</sub> (up to 10%), as is common for PcCo complexes [22,45,49]. Analysis of water-suppressed <sup>1</sup>H NMR spectra [50] showed no other soluble-reduced products (e.g., CH<sub>3</sub>OH, HCOOH, Figure S68–S70), which can be made by PcCo under certain conditions [24]. Analysis of the headspace from CPE experiments at selected loadings (Figure S67) shows Faradaic efficiencies in the range of 90 ± 10%, which is consistent with reports on similar PcCo catalysts [11,22,44,49,51].

### 2.6. Quantification of Electroactive <sup>RO</sup>PcCo

Integrated waves from cyclic voltammetry and differential pulse voltammetry experiments were used to assess the amount of electroactive <sup>RO</sup>PcCo deposited on graphite. The first redox event, near −0.1 V, was used in all cases. In general, the amount of electroactive compound was much lower than the amount deposited (Table 2). For some deposition concentrations for <sup>secBuO</sup>PcCo and for <sup>EtHexO</sup>PcCo, no waves could be detected by CV or DPV (Figure S61 for DPV traces). Based on our experiments, we estimate upper limit of ca. 1 × 10<sup>−14</sup> mol cm<sup>−2</sup> for those depositions using lower concentration.

## 3. Discussion

The three 1,4,8,11,15,18,22,25-octaalkoxyphthalocyanine Co(II) complexes feature a common <sup>RO</sup>PcCo core, but different ancillary alkoxy groups. Thus, while largely maintaining the electronic structure of the Co site, the nature of the alkoxy groups is a determinant of CO<sub>2</sub> reduction activity. Heterogeneous preparations of the three complexes can reduce CO<sub>2</sub> to CO at about the same overpotential, but their individual behaviors differ. This was first observed in their solution behavior. The bulky 2-ethylhexoxy group in <sup>EtHexO</sup>PcCo was introduced to promote solubility and prevent aggregation, but this complex showed an unexpected degree of solution aggregation based on its UV-vis spectra. <sup>EtHexO</sup>PcCo was generally less effective for CO<sub>2</sub> reduction and showed less reproducible results. One hypothesis is that non-specific aggregation of <sup>EtHexO</sup>PcCo during the evaporation process of a drop cast film is the reason for its uneven catalytic activity.

X-ray structures of <sup>nBuO</sup>PcCo and <sup>secBuO</sup>PcCo are known [39] and inspection of those structures allows us to form some hypotheses about their observed electrochemical behaviors. We note that attempts to produce X-ray quality crystals for <sup>EtHexO</sup>PcCo have proven unsuccessful in our labs. The structure of <sup>nBuO</sup>PcCo shows a Pc macrocycle that is slightly distorted from planarity, with an angle of about 22°, as defined by the angle of intersection between the planes defined by opposing isoindoline units. A planar molecule has an angle of 0° using this definition. In the solid state, the <sup>n</sup>butoxy groups point away from the ring in a staggered manner that results in the ring distortion. In contrast, the <sup>sec</sup>-butoxy groups cause a larger distortion from planarity (~38°). The <sup>sec</sup>-butoxy groups also are oriented in such a way that they point above and below the ring system. These distortions are likely the source of the slightly lower reduction potentials (Table 1) for <sup>secBuO</sup>PcCo than for <sup>nBuO</sup>PcCo. Based on those potentials, it is likely that <sup>EtHexO</sup>PcCo also has a distorted core. The distorted core, and the bulk from the alkoxy groups, also can insulate those <sup>RO</sup>PcCo from the electrode's surface and give rise to less prominent voltametric features. The inefficient packing of the bulky hydrophobic groups also could contribute to larger capacitive currents [52,53].

In addition to the ring distortions described above, the structure of <sup>nBuO</sup>PcCo suggests that the Co(II) ions can bind the butoxy (ether) oxygen on adjacent molecules (d(Co–O) = 2.370(4) Å and 2.424(5) Å) to generate a five-coordinate Co(II) center, potentially blocking Co active sites. Likewise, such interactions can promote more regular structures/packing that lower the level of dispersity. Metal–O–butoxy interactions have been observed in other systems too, although the M–O bonds are longer (3.26 Å to 3.37 Å) [36,54]. In other studies, it has been demonstrated that axial coordination via the stronger field ligand pyridine is known to modulate the activity of related PcCo systems [49,51]. In

contrast to  ${}^{\text{nBuO}}\text{PcCo}$ , the structure of  ${}^{\text{secBuO}}\text{PcCo}$  does not show such O-Co bonds in the solid state.

The relative performance of each catalyst is not simple to benchmark using a single metric. While FOWA is considered state of the art for determining kinetics, the variability in the performance of preparations limits the conclusions that we can draw from rate data alone. In general,  ${}^{\text{nBuO}}\text{PcCo}$  showed the most well-defined currents, both under Ar and under  $\text{CO}_2$  atmospheres. Based on relative current densities ( $i_p/i_0$ ),  ${}^{\text{secBuO}}\text{PcCo}$  shows the greatest enhancement at the lowest loading concentration and it shows fairly consistent current increases as a function of loading concentration. In contrast,  ${}^{\text{nBuO}}\text{PcCo}$  is a better performing catalyst based on absolute CV current densities. However,  ${}^{\text{secBuO}}\text{PcCo}$  and  ${}^{\text{EtHexO}}\text{PcCo}$  also performed comparably using this metric under some circumstances (e.g., CPE current densities at low loadings).

The mechanism of  $\text{CO}_2$  reduction by PcCo electrocatalysts has been discussed extensively [10,19,22,45,51]. The two widely implicated mechanisms involve: (1)  $\text{CO}_2$  activation by a  $1e^-$  reduced complex, which is formally Co(I) [22], or (2)  $\text{CO}_2$  activation by a  $2e^-$  reduced complex, which is formally Co(0) [45].  $\text{CO}_2$  binding in the Co(0) mechanism could involve a [Co(I)-H] intermediate, which has been proposed for the more electron-rich  ${}^{\text{nBuO}}\text{PcCo}$  complex [45]. In contrast, the parent PcCo is proposed to reduce  $\text{CO}_2$  via the  $1e^-$  (Co(I)) pathway [22,55]. Given these past observations and the CVs collected in this work showing an initial reduction followed by a second reduction at which catalytic currents are observed, an EECC mechanism (corresponding to electrochemical-electrochemical-chemical-chemical steps) is indicated in this work [45].

Given the probable EECC mechanism, foot-of-the-wave analysis (FOWA) [56,57] was used to probe the  $\text{CO}_2$  reduction kinetics. FOWA has emerged as a popular and useful method for understanding electrocatalyst kinetics when canonical “S-shaped” voltametric responses are not observed [56–59]. Recent work showed that a slightly modified FOWA is suitable for understanding the kinetics of heterogeneous electrocatalysis [60]. Specifically, the FOWA treatment is only slightly modified since the electroactive species is measured directly via integration of CVs; catalyst diffusion needs not be considered. FOW plots are set out in the Supporting Information (Figures S71–S79) and the rate constants are in Table 2. Note that FOWA is not presented for the cases where determination of the electroactive concentration was not possible.

Consistent with a recent report on unmodified PcCo, we observe the largest rate constants at the lowest catalyst-loading concentrations [22]. Most of the FOW rate constants (equivalently,  $\text{TOF}_{\text{max}}$  [60]) are on the order of  $10^2 \text{ s}^{-1}$ , also consistent with reported values [22]. However, some of the rate constants are over  $10^3 \text{ s}^{-1}$ , a factor of 10 larger than for PcCo. One hypothesis is that the higher dispersity of these compounds facilitates  $\text{CO}_2$  reduction kinetics by increasing per site activity [22,35]. We note, however, that the catalysts with bulkier substituents tend to have lower apparent electroactive concentrations, which could artificially increase the calculated rate constants when using FOWA. To test this, we used catalytic plateau current analysis, which is another way to extract turnover kinetics [58,61]. Plateau current analysis uses a ratio of currents with and without substrate in such a way that the absolute electroactive species concentration needs not be quantified. However, the rate constants can be influenced by substrate depletion or other side phenomena [56,58,61] and are used here only in a qualitative sense. The values are set out in the Supporting Information and range from 30 to  $600 \text{ s}^{-1}$  (Table S4). These values are in crude agreement with the  $k_{\text{FOW}}$  values, albeit smaller in magnitude. The agreement between rate constants from the two methods suggests that the kinetics values from FOWA are reliable as applied in this work.

Inspection of the different  $\text{CO}_2$  reduction rate constants (Table 2, Figure 4) reveals differences between the maximum current density ( $i_p/i_0$ ) and the rate constants calculated from FOWA. The  ${}^{\text{RO}}\text{PcCo}$  with the bulky sec-butoxy and 2-ethylhexoxy groups show larger rate constants than for  ${}^{\text{nBuO}}\text{PcCo}$ , but the values of  $i_p/i_0$  are similar. This behavior could be due to mass transport limitations that arise from analyzing peak currents. In

general, such phenomena are accounted for in FOWA by determining rate constants at lower overpotentials/current densities. Overall, these results suggest that  $n\text{Bu}^{\text{O}}\text{PcCo}$  is able to form better electroactive interactions with the electrode, but is a slower catalyst. The bulky *sec*-butoxy groups appear to give the best compromise between a good density of electroactive sites (alternatively, per site activity) and fast  $\text{CO}_2$  reduction kinetics. Such behavior contrasting could be due to the molecular structures of the catalysts or how they are deposited in the films.

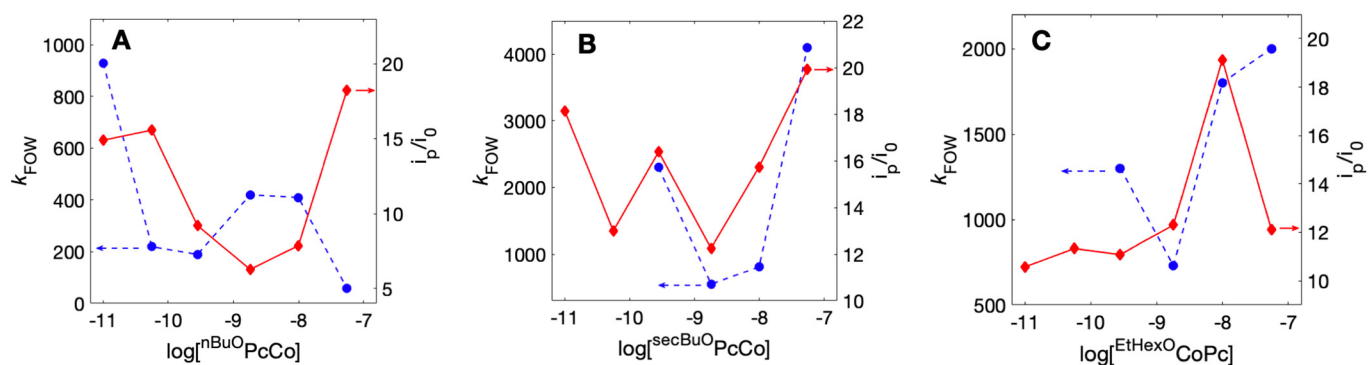


**Figure 4.** Comparisons of  $\text{CO}_2$  reduction rate constants from FOW analysis (left x-axes) and the ratios of observed currents and maximum catalytic currents ( $i_p/i_0$ , right y-axes) for  $n\text{Bu}^{\text{O}}\text{PcCo}$  (A),  $\text{secBu}^{\text{O}}\text{PcCo}$  (B), and  $\text{EtHex}^{\text{O}}\text{CoPc}$  (C).

Finally, the catalyst preparations studied here should be contrasted with other examples from the literature. First, there remains some debate about the use of deposited surface concentrations versus electroactive catalyst concentrations in the evaluation of  $\text{CO}_2$  reduction metrics (e.g., TOF) [22,49]. In some cases, neither approach is appropriate since the adsorbed molecular electrocatalysts can act similarly to metallic electrodes [48]. In our case, the simplicity of the drop cast method using soluble catalysts avoids limitations due to encapsulation or embedded sites and our results further demonstrate that there can be very large differences between deposited and electroactive catalyst concentrations. What is not yet clear is if electroactive species are the same under inert and  $\text{CO}_2$  atmospheres. In this work, both values are reported in Table 2, but electroactive concentration values are used to calculate  $\text{TOF}_{\text{max}}$  values. A benefit of FOWA is that it uses the low current regime of voltammograms, and therefore, is not subject to complicating factors (e.g., substrate/product diffusion). However, if we compute TOF from the CPE data, and use  $n\text{Bu}^{\text{O}}\text{PcCo}$  as an example case, we arrive at values of ca.  $40 \text{ s}^{-1}$  (based on electroactive concentrations) or  $0.1 \text{ s}^{-1}$  (based on deposited concentration). These values are in agreement with several different preparations of unfunctionalized  $\text{PcCo}$  [22,23,49] and demonstrate that functionalization with solubilizing groups does not appreciably affect the catalytic performance  $\text{CO}_2$  reduction. The one drawback to note is that slightly higher overpotentials are required when using  $\text{RO}^{\text{O}}\text{PcCo}$ , which we attribute to the electron-donating alkoxy groups.

## 4. Materials and Methods

### 4.1. General Materials and Methods

Synthetic manipulations were performed under  $\text{N}_2$  atmosphere using standard Schlenk techniques. Toluene and THF were distilled from sodium/benzophenone solution under  $\text{N}_2$  atmosphere. All other reagents were purchased from Sigma-Aldrich unless stated otherwise and used without further purification. Gases were from Praxair Canada. The 3,6-bis(2-ethylhexoxy)phthalonitrile, 1,4,8,11,15,18,22,25-octa(*n*-butoxy)phthalocyanine and octa(*sec*-butoxy)phthalocyanine  $\text{Co(II)}$  complexes were prepared according to modified literature procedures [36,62–64]. Additional details are given in the Supporting Information.

NMR spectra were acquired using Bruker Advance III spectrometers (400 MHz or 500 MHz). Electronic absorption spectra were recorded on a Cary 100-Bio spectropho-

tometer Gas chromatography (GC) experiments were performed using an Agilent 6890 gas chromatograph equipped with a Restek ShinCarbon ST Micropacked column and a thermal conductivity detector. Matrix-assisted laser desorption ionization time-of-flight mass spectrometry (MALDI-TOF-MS) data were collected with a Bruker Autoflex Speed spectrometer (Bruker Daltonics, Bremen, Germany) equipped with a 1 kHz Smartbeam-II laser. All samples were analyzed from dried droplets (i.e., without an added matrix). Positive-ion mass spectra were acquired typically within the  $m/z$  300–7000 range.

#### 4.2. Synthesis

1,4,8,11,15,18,22,25-Octakis(2-ethylhexoxy)-phthalocyanine ( $^{\text{EtHexO}}\text{PcH}_2$ ). The new ligand  $^{\text{EtHexO}}\text{PcH}_2$  was prepared using an appropriately modified literature procedure. 3,6-(2-Ethylhexoxy)phthalonitrile (1 g, 2.60 mmol) was dissolved in 15 mL of dry 2-ethylhexanol under an inert atmosphere and heated to 140 °C. While stirring, 40 mg (5.76 mmol) of  $\text{Li}_{(s)}$  was added to the solution and was left to react for 50 min. Upon cooling, the product was precipitate with addition of water and filtered over Celite. The product was extracted with  $\text{CH}_2\text{Cl}_2$ , and purified over silica with a 1:9 acetone: $\text{CH}_2\text{Cl}_2$  mobile phase. Yield 475 mg (47.5 %). UV-vis ( $\text{CH}_2\text{Cl}_2$ ): Q-band 771 nm, B-band 330 nm.  $^1\text{H}$  NMR  $\text{CDCl}_3$  (ppm): 7.14 (8H, s), 3.93 (16H, dd,  $J = 5.5$  Hz, 2.1 Hz), 1.77 (8H, hept,  $J = 6.2$  Hz), 1.51 (16H, m, dq,  $J = 14.9$  Hz, 7.5 Hz), 1.44 (16H, m), 1.32 (32H, m), 0.93 (24H, t,  $J = 7.5$  Hz), 0.90 (24H, t,  $J = 7.0$  Hz). MALDI-TOF MS: 1539.04 ( $\text{M}^+$ ) (calc: 1539.13)

1,4,8,11,15,18,22,25-Octakis(2-ethylhexoxy)-phthalocyanine cobalt ( $^{\text{EtHexO}}\text{PcCo}$ ). The ligand  $^{\text{EtHexO}}\text{PcH}_2$  (600 mg, 0.399 mmol) was dissolved in 30 mL of DMF and heated to 100 °C. 679 mg (2.73 mmol) of  $\text{Co}(\text{CH}_3\text{COO})_2 \cdot 4\text{H}_2\text{O}$  was added to the solution and it was stirred for 2 h at 100 °C. The  $^{\text{EtHexO}}\text{PcCo}$  was precipitated with addition of water, filtered, extracted with  $\text{CH}_2\text{Cl}_2$ , and purified over silica with a 1:20 acetone: $\text{CH}_2\text{Cl}_2$  mobile phase. Yield 412 mg (66.2%). UV-vis ( $\text{CH}_2\text{Cl}_2$ ): Q-band 741 nm, B-band 322 nm. MALDI-TOF MS: 1596.477 ( $\text{M}^+$ ) (calc: 1596.04)

#### 4.3. Electrochemical Methods

Basal-plane graphite (BPG) electrodes were prepared according to the literature [65]. Pyrolytic graphite was purchased from [www.graphitestore.com](http://www.graphitestore.com), accessed on 15 December 2022. Loctite Hysol 9460 epoxy was obtained from McMaster-Carr and silver paint was from SPI Supplies. All electrochemical experiments were conducted on a CH Instruments 6171B potentiostat, using a conventional three-electrode cell with two BPG electrodes as working electrode (3 mm  $\times$  3 mm) and counter electrode (3 mm  $\times$  3 mm). Aqueous electrochemistry used a Ag/AgCl reference in saturated KCl and potentials are reported with respect to the normal hydrogen electrode (NHE). Non-aqueous electrochemistry employed benzonitrile as a solvent with 0.1 M  $^n\text{Bu}_4\text{NPF}_6$  as electrolyte. The reference electrode was silver wire + 0.01 M  $\text{AgNO}_3$  in acetonitrile and potentials are reported versus the ferrocenium/ferrocene couple. All the cyclic voltammetry (CV) experiments were recorded at a 100  $\text{mV s}^{-1}$  scan rate unless otherwise noted. Working electrode surfaces were prepared by lightly abrading with wet sandpaper in a water and alumina slurry, washing thoroughly with deionized  $\text{H}_2\text{O}$  and acetone and drying by air flow, followed by sonication ( $\leq 5$  min) in acetonitrile (MeCN), and briefly drying with air flow and heat gun.

For heterogeneous electrochemical experiments, volumes of 5  $\mu\text{L}$  of toluene solutions of  $^{\text{RO}}\text{PcCo}$  catalysts were drop-cast onto BPG. Catalyst-absorbed electrodes were gently rinsed with deionized  $\text{H}_2\text{O}$  to remove loosely bound material and the surfaces were dried prior to electrochemical experiments. All aqueous electrochemistry experiments used a 0.1 M KCl solution at adjusted pH of 4.5 before the electrolysis.

## 5. Conclusions

A series of solution processable 1,4,8,11,15,18,22,25-octaalkoxyphthalocyanine Co(II) complexes were produced and investigated for their electrocatalytic  $\text{CO}_2$ -to-CO conversion properties. Importantly, the addition of solubilizing groups does not dramatically affect

catalyst selectivity or TOF values with respect to the parent PcCo. This contrasts with other electrocatalyst preparations that can strongly affect both kinetics and selectivity, as demonstrated for O<sub>2</sub> reduction [66]. Our experiments, using a solution-deposited catalyst, suggest that catalyst aggregation still must be considered with respect to kinetics, even in cases where bulky groups have been added to the PcCo scaffold to promote solubility, as is the case for EtHex<sup>O</sup>PcCo. Improvements in catalyst kinetics are possible via incorporation of bulk peripheral substituents (i.e., nBu<sup>O</sup>PcCo versus secBu<sup>O</sup>PcCo), which discourages intermolecular Co-O bond formation. What is not yet clear is how the degree of bulk in the ancillary groups can affect other properties of films, such as porosity.

The concepts described here are important for connecting the behavior of different catalyst preparations (e.g., ref. [22] versus [49]) in the search for a heterogeneous CO<sub>2</sub> conversion catalyst preparation with the best activity per site and per unit area. One important challenge in the development of CO<sub>2</sub> reduction catalysts (or any electrocatalyst, for that matter) is maximizing the activity, availability, and density of active sites. Encapsulation in polymers or physical dispersion has been successful, but the solution processability of the complexes presented here adds a potential route for better preparations. While drop casting is unlikely to be a suitable approach for the production of practical devices, a combination of other immobilization approaches with our soluble catalysts is of interest. Based on our results, simple modifications to encourage dispersion (e.g., via alkylation) can be helpful, but only to a point. This is evinced by the relatively poorer performance of the catalyst with the bulkiest groups, EtHex<sup>O</sup>PcCo. Further investigations into how catalyst designs can improve dispersion and per site activity are needed.

**Supplementary Materials:** The following supporting information can be downloaded at: <https://www.mdpi.com/article/10.3390/inorganics11010043/s1>, Experimental Details and Syntheses (Figure S1), Optical Spectra (Figure S2), Full Cyclic Voltammetry Data in Triplicate (Figures S3–S60), Differential Pulse Voltammetry (Figure S61), Scan Rate Analysis (Figures S62 and S63), Current Response Versus Loading Analysis (Tables S1 and S2, Figures S64 and S65), Foot-of-the-Wave Analyses (Table S3, Figures S66–S74), Plateau Current Analysis (Table S4), Catalyst Stability Tests (Figures S75 and S76) [67–70].

**Author Contributions:** Conceptualization, D.B.L. and J.J.W.; methodology, J.J.W. and D.B.L.; formal analysis, E.T. and D.M.; investigation, E.T. and D.M.; writing—original draft preparation, E.T., D.M., J.J.W. and D.B.L.; writing—review and editing, E.T., D.M., J.J.W. and D.B.L.; supervision, D.B.L. and J.J.W.; project administration, D.B.L. and J.J.W.; funding acquisition, D.B.L. and J.J.W. All authors have read and agreed to the published version of the manuscript.

**Funding:** This research was funded by the Natural Sciences and Engineering Research Council (NSERC) of Canada (Discovery Grant Program, RGPIN 06272 to JJW and RGPIN 05800 to DBL) and by Simon Fraser University.

**Data Availability Statement:** Data are available upon request.

**Conflicts of Interest:** The authors declare no conflict of interest. The funders had no role in the design of the study; in the collection, analyses, or interpretation of data; in the writing of the manuscript; or in the decision to publish the results.

## References

1. Whipple, D.T.; Kenis, P.J.A. Prospects of CO<sub>2</sub> Utilization via Direct Heterogeneous Electrochemical Reduction. *J. Phys. Chem. Lett.* **2010**, *1*, 3451–3458. [[CrossRef](#)]
2. Jouny, M.; Luc, W.; Jiao, F. General Techno-Economic Analysis of CO<sub>2</sub> Electrolysis Systems. *Ind. Eng. Chem. Res.* **2018**, *57*, 2165–2177. [[CrossRef](#)]
3. Bushuyev, O.S.; De Luna, P.; Dinh, C.T.; Tao, L.; Saur, G.; van de Lagemaat, J.; Kelley, S.O.; Sargent, E.H. What Should We Make with CO<sub>2</sub> and How Can We Make It? *Joule* **2018**, *2*, 825–832. [[CrossRef](#)]
4. De Luna, P.; Hahn, C.; Higgins, D.; Jaffer, S.A.; Jaramillo, T.F.; Sargent, E.H. What Would It Take for Renewably Powered Electrosynthesis to Displace Petrochemical Processes? *Science* **2019**, *364*, eaav3506. [[CrossRef](#)] [[PubMed](#)]
5. Smith, W.A.; Burdyny, T.; Vermaas, D.A.; Geerlings, H. Pathways to Industrial-Scale Fuel Out of Thin Air from CO<sub>2</sub> Electrolysis. *Joule* **2019**, *3*, 1822–1834. [[CrossRef](#)]

6. Keith, D.W.; Holmes, G.; Angelo, D.S.; Heidel, K. A Process for Capturing CO<sub>2</sub> from the Atmosphere. *Joule* **2018**, *2*, 1573–1594. [[CrossRef](#)]
7. Nitopi, S.; Bertheussen, E.; Scott, S.B.; Liu, X.; Engstfeld, A.K.; Horch, S.; Seger, B.; Stephens, I.E.L.; Chan, K.; Hahn, C.; et al. Progress and Perspectives of Electrochemical CO<sub>2</sub> Reduction on Copper in Aqueous Electrolyte. *Chem. Rev.* **2019**, *119*, 7610–7672. [[CrossRef](#)]
8. Torbensen, K.; Boudy, B.; Joulié, D.; von Wolff, N.; Robert, M. Emergence of CO<sub>2</sub> Electrolyzers Including Supported Molecular Catalysts. *Curr. Opin. Electrochem.* **2020**, *24*, 49–55. [[CrossRef](#)]
9. Liu, X.; Xiao, J.; Peng, H.; Hong, X.; Chan, K.; Nørskov, J.K. Understanding Trends in Electrochemical Carbon Dioxide Reduction Rates. *Nat. Commun.* **2017**, *8*, 15438. [[CrossRef](#)]
10. Manbeck, G.F.; Fujita, E. A Review of Iron and Cobalt Porphyrins, Phthalocyanines and Related Complexes for Electrochemical and Photochemical Reduction of Carbon Dioxide. *J. Porphyr. Phthalocya.* **2015**, *19*, 45–64. [[CrossRef](#)]
11. Corbin, N.; Zeng, J.; Williams, K.; Manthiram, K. Heterogeneous Molecular Catalysts for Electrocatalytic CO<sub>2</sub> Reduction. *Nano Res.* **2019**, *12*, 2093–2125. [[CrossRef](#)]
12. Zhang, R.; Warren, J.J. Recent Developments in Metalloporphyrin Electrocatalysts for Reduction of Small Molecules: Strategies for Managing Electron and Proton Transfer Reactions. *ChemSusChem* **2021**, *14*, 293–302. [[CrossRef](#)] [[PubMed](#)]
13. Usman, M.; Humayun, M.; Garba, M.D.; Ullah, L.; Zeb, Z.; Helal, A.; Suliman, M.H.; Alfaifi, B.Y.; Iqbal, N.; Abdinejad, M.; et al. Electrochemical Reduction of CO<sub>2</sub>: A Review of Cobalt Based Catalysts for Carbon Dioxide Conversion to Fuels. *Nanomaterials* **2021**, *11*, 2029. [[CrossRef](#)]
14. Sun, L.; Reddu, V.; Fisher, A.C.; Wang, X. Electrocatalytic Reduction of Carbon Dioxide: Opportunities with Heterogeneous Molecular Catalysts. *Energy Environ. Sci.* **2020**, *13*, 374–403. [[CrossRef](#)]
15. Wu, Y.; Liang, Y.; Wang, H. Heterogeneous Molecular Catalysts of Metal Phthalocyanines for Electrochemical CO<sub>2</sub> Reduction Reactions. *Acc. Chem. Res.* **2021**, *54*, 3149–3159. [[CrossRef](#)] [[PubMed](#)]
16. Lin, S.; Diercks, C.S.; Zhang, Y.-B.; Kornienko, N.; Nichols, E.M.; Zhao, Y.; Paris, A.R.; Kim, D.; Yang, P.; Yaghi, O.M.; et al. Covalent Organic Frameworks Comprising Cobalt Porphyrins for Catalytic CO<sub>2</sub> Reduction in Water. *Science* **2015**, *349*, 1208–1213. [[CrossRef](#)] [[PubMed](#)]
17. Diercks, C.S.; Lin, S.; Kornienko, N.; Kapustin, E.A.; Nichols, E.M.; Zhu, C.; Zhao, Y.; Chang, C.J.; Yaghi, O.M. Reticular Electronic Tuning of Porphyrin Active Sites in Covalent Organic Frameworks for Electrocatalytic Carbon Dioxide Reduction. *J. Am. Chem. Soc.* **2018**, *140*, 1116–1122. [[CrossRef](#)] [[PubMed](#)]
18. Wang, D.-G.; Qiu, T.; Guo, W.; Liang, Z.; Tabassum, H.; Xia, D.; Zou, R. Covalent Organic Framework-Based Materials for Energy Applications. *Energy Environ. Sci.* **2021**, *14*, 688–728. [[CrossRef](#)]
19. Abe, T.; Imaya, H.; Yoshida, T.; Tokita, S.; Schlettwein, D.; Wöhrle, D.; Kaneko, M. Electrochemical CO<sub>2</sub> Reduction Catalysed by Cobalt Octacyanophthalocyanine and Its Mechanism. *J. Porphyr. Phthalocya.* **1997**, *1*, 315–321. [[CrossRef](#)]
20. Lieber, C.M.; Lewis, N.S. Catalytic Reduction of Carbon Dioxide at Carbon Electrodes Modified with Cobalt Phthalocyanine. *J. Am. Chem. Soc.* **1984**, *106*, 5033–5034. [[CrossRef](#)]
21. Kapusta, S.; Hackerman, N. Carbon Dioxide Reduction at a Metal Phthalocyanine Catalyzed Carbon Electrode. *J. Electrochem. Soc.* **1984**, *131*, 1511–1514. [[CrossRef](#)]
22. Zhu, M.; Ye, R.; Jin, K.; Lazouski, N.; Manthiram, K. Elucidating the Reactivity and Mechanism of CO<sub>2</sub> Electroreduction at Highly Dispersed Cobalt Phthalocyanine. *ACS Energy Lett.* **2018**, *3*, 1381–1386. [[CrossRef](#)]
23. Zhang, X.; Wu, Z.; Zhang, X.; Li, L.; Li, Y.; Xu, H.; Li, X.; Yu, X.; Zhang, Z.; Liang, Y.; et al. Highly Selective and Active CO<sub>2</sub> Reduction Electrocatalysts Based on Cobalt Phthalocyanine/Carbon Nanotube Hybrid Structures. *Nat. Commun.* **2017**, *8*, 14675. [[CrossRef](#)] [[PubMed](#)]
24. Boutin, E.; Wang, M.; Lin, J.C.; Mesnage, M.; Mendoza, D.; Lassalle-Kaiser, B.; Hahn, C.; Jaramillo, T.F.; Robert, M. Aqueous Electrochemical Reduction of Carbon Dioxide and Carbon Monoxide into Methanol with Cobalt Phthalocyanine. *Angew. Chem. Int. Ed.* **2019**, *58*, 16172–16176. [[CrossRef](#)]
25. Wu, Y.; Jiang, Z.; Lu, X.; Liang, Y.; Wang, H. Domino Electroreduction of CO<sub>2</sub> to Methanol on a Molecular Catalyst. *Nature* **2019**, *575*, 639–642. [[CrossRef](#)]
26. Hu, X.-M.; Rønne, M.H.; Pedersen, S.U.; Skrydstrup, T.; Daasbjerg, K. Enhanced Catalytic Activity of Cobalt Porphyrin in CO<sub>2</sub> Electroreduction upon Immobilization on Carbon Materials. *Angew. Chem. Int. Ed.* **2017**, *56*, 6468–6472. [[CrossRef](#)]
27. Ren, S.; Joulié, D.; Salvatore, D.; Torbensen, K.; Wang, M.; Robert, M.; Berlinguette, C.P. Molecular Electrocatalysts Can Mediate Fast, Selective CO<sub>2</sub> Reduction in a Flow Cell. *Science* **2019**, *365*, 367–369. [[CrossRef](#)] [[PubMed](#)]
28. Wang, M.; Torbensen, K.; Salvatore, D.; Ren, S.; Joulié, D.; Dumoulin, F.; Mendoza, D.; Lassalle-Kaiser, B.; Işci, U.; Berlinguette, C.P.; et al. CO<sub>2</sub> Electrochemical Catalytic Reduction with a Highly Active Cobalt Phthalocyanine. *Nat. Commun.* **2019**, *10*, 3602. [[CrossRef](#)]
29. Ghani, F.; Kristen, J.; Riegler, H. Solubility Properties of Unsubstituted Metal Phthalocyanines in Different Types of Solvents. *J. Chem. Eng. Data* **2012**, *57*, 439–449. [[CrossRef](#)]
30. Snow, A.W. Phthalocyanine Aggregation. In *The Porphyrin Handbook: Phthalocyanines: Properties and Materials*; Elsevier Inc.: Amsterdam, The Netherlands, 2003; Volume 17, pp. 129–176. ISBN 9780123932273.
31. Wu, Y.; Hu, G.; Rooney, C.L.; Brudvig, G.W.; Wang, H. Heterogeneous Nature of Electrocatalytic CO/CO<sub>2</sub> Reduction by Cobalt Phthalocyanines. *ChemSusChem* **2020**, *13*, 6296–6299. [[CrossRef](#)]

32. Durmuş, M.; Nyokong, T. Synthesis and Solvent Effects on the Electronic Absorption and Fluorescence Spectral Properties of Substituted Zinc Phthalocyanines. *Polyhedron* **2007**, *26*, 2767–2776. [[CrossRef](#)]
33. Bayar, Ş.; Dınçer, H.A.; Uğur, A.L. Novel Non-Aggregated Soluble Metallophthalocyanines Bearing Carboxylic Acid Groups. *J. Coord. Chem.* **2012**, *65*, 1371–1380. [[CrossRef](#)]
34. Biyiklioglu, Z.; Alp, H. Synthesis, Characterization, Electropolymerization and Aggregation Properties of Axially Diethyl-Dimethylaminophenoxypropanoxy Substituted Silicon Phthalocyanines and Their Water Soluble Derivatives. *Dye. Pigment.* **2016**, *132*, 213–222. [[CrossRef](#)]
35. Choi, J.; Wagner, P.; Gambhir, S.; Jalili, R.; MacFarlane, D.R.; Wallace, G.G.; Officer, D.L. Steric Modification of a Cobalt Phthalocyanine/Graphene Catalyst to Give Enhanced and Stable Electrochemical CO<sub>2</sub> Reduction to CO. *ACS Energy Lett.* **2019**, *4*, 666–672. [[CrossRef](#)]
36. McKearney, D.; Zhou, W.; Zellman, C.; Williams, V.E.; Leznoff, D.B. Facile Tuning of Strong Near-IR Absorption Wavelengths in Manganese(III) Phthalocyanines via Axial Ligand Exchange. *Chem. Commun.* **2019**, *55*, 6696–6699. [[CrossRef](#)] [[PubMed](#)]
37. McKeown, N.B.; Chambrier, I.; Cook, M.J. Synthesis and Characterisation of Some 1,4,8,11,15,18,22,25-Octa-Alkyl- and 1,4,8,11,15,18-Hexa-Alkyl-22,25-Bis(Carboxypropyl)Phthalocyanines. *J. Chem. Soc., Perkin Trans. 1* **1990**, *0*, 1169–1177. [[CrossRef](#)]
38. Furuyama, T.; Uchiyama, S.; Iwamoto, T.; Maeda, H.; Segi, M. Changes of Phthalocyanine Visible Color Caused by Near-IR Solvatochromism. *J. Porphy. Phthalocyanines* **2018**, *22*, 88–94. [[CrossRef](#)]
39. Roshea, D. *Manipulating the Electronic Properties of Metallophthalocyanines through Interactions with the Ligand's Aromatic Core*; Simon Fraser University: Burnaby, BC, Canada, 2022.
40. Tolbin, A.Y.; Pushkarev, V.E.; Sedova, M.V.; Maklakov, S.S.; Tomilova, L.G. Aggregation of Slipped-Cofacial Phthalocyanine J-Type Dimers: Spectroscopic and AFM Study. *Spectrochim. Acta A Mol. Biomol. Spectrosc.* **2018**, *205*, 335–340. [[CrossRef](#)]
41. Balaban, T.S. Tailoring Porphyrins and Chlorins for Self-Assembly in Biomimetic Artificial Antenna Systems. *Acc. Chem. Res.* **2005**, *38*, 612–623. [[CrossRef](#)]
42. Charalambidis, G.; Georgilis, E.; Panda, M.K.; Anson, C.E.; Powell, A.K.; Doyle, S.; Moss, D.; Jochum, T.; Horton, P.N.; Coles, S.J.; et al. A Switchable Self-Assembling and Disassembling Chiral System Based on a Porphyrin-Substituted Phenylalanine-Phenylalanine Motif. *Nat. Commun.* **2016**, *7*, 12657. [[CrossRef](#)]
43. Muto, T.; Temma, T.; Kimura, M.; Hanabusa, K.; Shirai, H. Elongation of the  $\pi$ -System of Phthalocyanines by Introduction of Thienyl Substituents at the Peripheral  $\beta$  Positions. Synthesis and Characterization. *J. Org. Chem.* **2001**, *66*, 6109–6115. [[CrossRef](#)]
44. Feng, Q.; Sun, Y.; Gu, X.; Dong, Z. Advances of Cobalt Phthalocyanine in Electrocatalytic CO<sub>2</sub> Reduction to CO: A Mini Review. *Electrocatalysis* **2022**, *13*, 675–690. [[CrossRef](#)]
45. Abe, T.; Taguchi, F.; Yoshida, T.; Tokita, S.; Schnurpfeil, G.; Wöhrle, D.; Kaneko, M. Electrocatalytic CO<sub>2</sub> Reduction by Cobalt Octabutoxyphthalocyanine Coated on Graphite Electrode. *J. Mol. Catal. A-Chem.* **1996**, *112*, 55–61. [[CrossRef](#)]
46. Durand, R.R.; Anson, F.C. Catalysis of Dioxygen Reduction at Graphite Electrodes by an Adsorbed Cobalt(II) Porphyrin. *J. Electroanal. Chem.* **1982**, *134*, 273–289. [[CrossRef](#)]
47. Song, E.; Shi, C.; Anson, F.C. Comparison of the Behavior of Several Cobalt Porphyrins as Electrocatalysts for the Reduction of O<sub>2</sub> at Graphite Electrodes. *Langmuir* **1998**, *14*, 4315–4321. [[CrossRef](#)]
48. Kaminsky, C.J.; Weng, S.; Wright, J.; Surendranath, Y. Adsorbed Cobalt Porphyrins Act like Metal Surfaces in Electrocatalysis. *Nat. Catal.* **2022**, *5*, 430–442. [[CrossRef](#)]
49. Kramer, W.W.; McCrory, C.C.L. Polymer Coordination Promotes Selective CO<sub>2</sub> Reduction by Cobalt Phthalocyanine. *Chem. Sci.* **2016**, *7*, 2506–2515. [[CrossRef](#)]
50. Simpson, A.J.; Brown, S.A. Purge NMR: Effective and Easy Solvent Suppression. *J. Magn. Reson.* **2005**, *175*, 340–346. [[CrossRef](#)]
51. Liu, Y.; McCrory, C.C.L. Modulating the Mechanism of Electrocatalytic CO<sub>2</sub> Reduction by Cobalt Phthalocyanine through Polymer Coordination and Encapsulation. *Nat. Commun.* **2019**, *10*, 1683. [[CrossRef](#)]
52. Dunwell, M.; Yan, Y.; Xu, B. Understanding the Influence of the Electrochemical Double-Layer on Heterogeneous Electrochemical Reactions. *Curr. Opin. Chem. Eng.* **2018**, *20*, 151–158. [[CrossRef](#)]
53. Uddin, M.S.; Tanaya Das, H.; Maiyalagan, T.; Elumalai, P. Influence of Designed Electrode Surfaces on Double Layer Capacitance in Aqueous Electrolyte: Insights from Standard Models. *Appl. Surf. Sci.* **2018**, *449*, 445–453. [[CrossRef](#)]
54. Jinwan, C.; Jundong, W.; Jinling, H.; Naisheng, C. The Ring-Substituted Phthalocyanines and Its Metal Complexes: Crystal Structure of 1,4,8,11,15,18,22,25-Octabutoxyphthalocyaninatocopper. *Chin. Sci. Bull.* **2002**, *47*, 3.
55. Yoshida, T.; Kamato, K.; Tsukamoto, M.; Iida, T.; Schlettwein, D.; Wöhrle, D.; Kaneko, M. Selective Electrocatalysis for CO<sub>2</sub> Reduction in the Aqueous Phase Using Cobalt Phthalocyanine/Poly-4-Vinylpyridine Modified Electrodes. *J. Electroanal. Chem.* **1995**, *385*, 209–225. [[CrossRef](#)]
56. Costentin, C.; Drouet, S.; Robert, M.; Savéant, J.-M. Turnover Numbers, Turnover Frequencies, and Overpotential in Molecular Catalysis of Electrochemical Reactions. Cyclic Voltammetry and Preparative-Scale Electrolysis. *J. Am. Chem. Soc.* **2012**, *134*, 11235–11242. [[CrossRef](#)] [[PubMed](#)]
57. Costentin, C.; Drouet, S.; Robert, M.; Savéant, J.-M. Correction to Turnover Numbers, Turnover Frequencies, and Overpotential in Molecular Catalysis of Electrochemical Reactions. Cyclic Voltammetry and Preparative-Scale Electrolysis. *J. Am. Chem. Soc.* **2012**, *134*, 19949–19950. [[CrossRef](#)]
58. Lee, K.J.; Elgrishi, N.; Kandemir, B.; Dempsey, J.L. Electrochemical and Spectroscopic Methods for Evaluating Molecular Electrocatalysts. *Nat. Rev. Chem.* **2017**, *1*, 1–4. [[CrossRef](#)]

59. Wang, V.C.-C.; Johnson, B.A. Interpreting the Electrocatalytic Voltammetry of Homogeneous Catalysts by the Foot of the Wave Analysis and Its Wider Implications. *ACS Catal.* **2019**, *9*, 7109–7123. [[CrossRef](#)]
60. Matheu, R.; Neudeck, S.; Meyer, F.; Sala, X.; Llobet, A. Foot of the Wave Analysis for Mechanistic Elucidation and Benchmarking Applications in Molecular Water Oxidation Catalysis. *ChemSusChem* **2016**, *9*, 3361–3369. [[CrossRef](#)] [[PubMed](#)]
61. Costentin, C.; Savéant, J.-M. Multielectron, Multistep Molecular Catalysis of Electrochemical Reactions: Benchmarking of Homogeneous Catalysts. *ChemElectroChem* **2014**, *1*, 1226–1236. [[CrossRef](#)]
62. Al-Raqa, S.Y. The Synthesis and Photophysical Properties of Novel, Symmetrical, Hexadecasubstituted Zn Phthalocyanines and Related Unsymmetrical Derivatives. *Dye. Pigment.* **2008**, *77*, 259–265. [[CrossRef](#)]
63. Gao, D.; Xu, H.; Yan, T.; Peng, B. The Synthesis of Symmetrically Octa-Substituted Phthalocyanines and Their Physical and Photo-Physical Properties. *J. Chin. Chem. Soc.* **2001**, *48*, 1189–1196. [[CrossRef](#)]
64. Attia, M.S.; Ali, K.; El-Kemary, M.; Darwish, W.M. Phthalocyanine-Doped Polystyrene Fluorescent Nanocomposite as a Highly Selective Biosensor for Quantitative Determination of Cancer Antigen 125. *Talanta* **2019**, *201*, 185–193. [[CrossRef](#)] [[PubMed](#)]
65. Hanson, S.S.; Warren, J.J. Syntheses, Characterization, and Electrochemical Behavior of Alkylated 2-(2'-Quinoly)benzimidazole) Complexes of Rhenium (I). *Can. J. Chem.* **2017**, *96*, 119–123. [[CrossRef](#)]
66. Rigsby, M.L.; Wasylenko, D.J.; Pegis, M.L.; Mayer, J.M. Medium Effects Are as Important as Catalyst Design for Selectivity in Electrocatalytic Oxygen Reduction by Iron-Porphyrin Complexes. *J. Am. Chem. Soc.* **2015**, *137*, 4296–4299. [[CrossRef](#)] [[PubMed](#)]
67. Forsyth, T.P.; Bradley, D.; Williams, G.; Montalban, A.G.; Stern, C.L.; Barrett, A.G.M.; Hoffman, B.M. A Facile and Regioselective Synthesis of Trans-Heterofunctionalized Porphyrazine Derivatives. *J. Org. Chem.* **1998**, *63*, 331–336. [[CrossRef](#)]
68. Cook, M.J.; Dunn, A.J.; Howe, S.D.; Thomson, A.J.; Harrison, K.J. Octa-Alkoxy Phthalocyanine and Naphthalocyanine Derivatives: Dyes with Q-Band Absorption in the Far Red or near Infrared. *J. Chem. Soc. Perkin Trans. 1* **1988**, *8*, 2453–2458. [[CrossRef](#)]
69. Abdelkader, A.M.; Cooper, A.J.; Dryfe R a, W.; Kinloch, I.A. How to Get between the Sheets: A Review of Recent Works on the Electrochemical Exfoliation of Graphene Materials from Bulk Graphite. *Nanoscale* **2015**, *7*, 6944–6956. [[CrossRef](#)]
70. Bard, A.J.; Faulkner LR Allen JBard Larry, R. Faulkner, *Electrochemical Methods: Fundamentals and Applications*, New York: Wiley, 2001, 2nd Ed. *Russ. J. Electrochem.* **2002**, *38*, 1364–1365. [[CrossRef](#)]

**Disclaimer/Publisher's Note:** The statements, opinions and data contained in all publications are solely those of the individual author(s) and contributor(s) and not of MDPI and/or the editor(s). MDPI and/or the editor(s) disclaim responsibility for any injury to people or property resulting from any ideas, methods, instructions or products referred to in the content.